Trajectory Design of a ~~Scramjet-Rocket Multi-Stage~~ Rocket-Scramjet-Rocket Launch System

Sholto O. Forbes-Spyratos[a], Michael P. Kearney[b], Michael K. Smart[c] and Ingo H. Jahn[d]
The University of Queensland, Queensland, Australia, 4072

The integration of a scramjet as one of the stages of a multi-stage launch system has the potential to allow for small payloads to be delivered cheaply and reusably to orbit. This paper determines the maximum payload to orbit trajectory of a ~~multi-stage~~ rocket-scramjet-rocket system. This trajectory has been calculated by formulating the problem as an optimal control problem, then solving it using the pseudospectral method. The optimal trajectory for the scramjet stage was found to be split into two parts: a constant dynamic pressure path and a pull-up manoeuvre. This pull up manoeuvre results in a 11.4% improvement in payload mass to orbit when compared to a constant dynamic pressure trajectory with no pull-up. ~~Fortuitously~~ Furthermore, this pull-up manoeuvre ~~also~~ decreases the maximum dynamic pressure experienced by the final rocket stage by 36.2%. The maximum dynamic pressure allowable for the scramjet was varied by ±5kPa and shown to produce only a +0.42% and −0.58% variation in the payload mass to orbit. The drag produced by the vehicle was increased by 10% and was shown to produce only minimal difference in the optimal trajectory, indicating that the solution is robust with variation in vehicle design.

13/6/16 What you do with the 3rd stage is still messy & unclear. There is also a need for clear definition of symbols, particularly the angles. Figs need to be near relevant text

[a] Ph.D. Candidate, Centre for Hypersonics, School of Mechanical and Mining Engineering. Member AIAA.
[b] Lecturer, School of Mechanical and Mining Engineering.
[c] Professor, Centre for Hypersonics, School of Mechanical and Mining Engineering. Senior Member AIAA.
[d] Lecturer, Centre for Hypersonics, School of Mechanical and Mining Engineering. Member AIAA.

Nomenclature

I_{sp}	=	Specific Impulse (s)	L_N	=	Legendre Polynomial
w_k	=	Weighting Function	D	=	Differentiation Matrix
t	=	Time	τ	=	Normalised Time Scale
N	=	Node Number	t	=	Time (s)
$\mathbf{x}$	=	Primal Variables	$\mathbf{u}$	=	Control Variables
			f, g, ψ,	=	Functions
q	=	Dynamic Pressure (Pa)	λ, M, P		
C	=	Cost Function	F	=	Force (N)
ρ	=	Density (kg/m^2)	c	=	Aerodynamic Coefficient
v	=	Velocity (m/s)	A	=	Reference Area (m^2)
H	=	Horizontal Position (m)	V	=	Vertical Position (m)
θ	=	Vehicle Orientation Angle (rad)	ω	=	Angular Velocity (rad/s)
a	=	Acceleration (m/s^2)	m	=	Mass (kg)
T	=	Thrust (N)	w_{cap}	=	Capture Width
Subscripts					
			2	=	2nd Stage Scramjet Vehicle
1	=	1st Stage Rocket			
3	=	3rd Stage Rocket	$\rightarrow$	=	Stage Transition
d	=	Drag	L	=	Lift
s	=	Specific	f	=	Fuel
$*$	=	Payload	LOX	=	Liquid Oxygen
LH2	=	Liquid Hydrogen			

I. Introduction

Currently most small satellite launches co-manifest with a larger payload, leaving their launch schedule and trajectory at the mercy of the major payload. The demand for small payload launches is increasing [1], driving the development of cheap and efficient launch systems for independent

launches of small payloads. A multi-stage launch system incorporating a scramjet second stage has been proposed as a dedicated small satellite launch vehicle [2]. Scramjets (supersonic combustion ramjets) are airbreathing engines that operate over Mach numbers in the hypersonic range [3]. Scramjet engines are a primary candidate for powering the next generation of small payload launch vehicles, producing higher specific impulse (I_{sp}) than rockets within their operating range and providing key operability benefits. These include increased flexibility of launch windows and an increased range of mission capabilities [4]. Scramjets can accelerate a launch vehicle without the need to carry oxidiser on board, providing weight savings compared to rocket-powered vehicles. The reduction of weight carried within the vehicle fuselage enables the integration of avionics and landing gear, allowing for the design of a reusable vehicle in the style of conventional aerospace vehicles. However, a launch system must contain engines capable of accelerating the scramjet to its operating speed and also placing the payload in orbit.

This paper presents a trajectory for a scramjet-rocket vehicle after first stage boost, designed using optimal control methods. This paper utilises a scramjet-rocket multi-stage launch system that has been proposed at the Centre for Hypersonics at The University of Queensland [2]. This launch system is delivered to a starting point by a first stage that is assumed to be able to achieve the necessary flight conditions for scramjet stage separation. In practice the first stage requires the use of a rocket or other accelerator, however for the purposes of this study the mode of acceleration before the scramjet stage is inconsequential.

The trajectory profile of multi-stage vehicles has typically been designed around the scramjet stage flying a constant dynamic pressure trajectory [5–7]. A constant dynamic pressure trajectory follows the maximum dynamic pressure that the scramjet powered vehicle is able to withstand structurally, ensuring maximum thrust production from the scramjet engines. Such a trajectory produces maximum acceleration from the scramjet stage but may not be globally optimal for the multi-stage system. A constant dynamic pressure trajectory may be suboptimal due to the separation of the final stage into a high dynamic pressure environment, at a potentially suboptimal trajectory angle. This may result in suboptimal performance of the final stage rocket and the inclusion of unnecessary design constraints.

Launch vehicles utilising rocket and airbreathing propulsion within a single stage have previously been shown to fly at maximum dynamic pressure for the majority of airbreathing operation, followed by a pull-up before airbreathing engine cut-off [8–10]. A pull-up produces an overall favourable trade-off by allowing for the airbreathing engines to be used to increase the altitude of the launch vehicle, with the downside of reducing the thrust of the airbreathing engine due to a lower mass flow rate into the engine. The increase in altitude and trajectory angle produced by a pull-up manoeuvre results in the rocket engines being ignited at higher altitude, allowing the rocket to operate with reduced drag. A trajectory involving a pull-up has been shown to be the optimal trajectory for vehicles where the rocket engines are not ignited until circularization altitude [8, 9] as well as vehicles where the rocket engine is ignited immediately after airbreathing engine cut-off [10].

For launch systems with airbreathing and rocket propulsion combined within a single stage, the pull-up manoeuvre is a simple trade-off between velocity and altitude. However, for the proposed scramjet-rocket multi-stage system, the scramjet stage and rocket stage are sequential and are separated completely. The resultant change in mass and aerodynamic characteristics adds to the complexity of the trajectory analysis. For a robust multi-stage trajectory design there is a trade-off between the high efficiency of the scramjet engine, the thrust produced, the energy necessary to increase the altitude of the scramjet stage, and the aerodynamic efficiency when performing the required direction change. A pull-up manoeuvre has previously been identified as having potential advantages for a multi-stage airbreathing-rocket system [11]. However, these advantages were observed in a suboptimal trajectory with variation in dynamic pressure throughout multiple modes of airbreathing engine operation. The inherent complexity of a multi-stage system delivering payload to orbit necessitates an investigation into the optimal launch trajectory design.

This paper utilises optimal control theory to generate the optimal trajectory path for a scramjet-rocket multi-stage vehicle. Optimal control theory allows a trajectory to be optimised in its entirety and has been widely used in aerospace applications for computing trajectories when there is a global objective to be optimised, such as minimum fuel or maximum payload delivery [12–14]. Optimal control is also extremely flexible, as the objective of the optimal control routine can be modified easily to investigate a range of trajectory targets [15]. Complex optimal control problems (such

as a highly nonlinear model of hypersonic flight) necessitate the use of direct methods such as direct single shooting, multiple shooting, or collocation. The pseudospectral collocation method of optimal control is utilised in this study due to its accuracy, efficiency, and radius of convergence when compared to other optimal control techniques [16, 17].

The remainder of the paper is as follows: Section II presents models of the scramjet and rocket stages, including the engine models. Section III presents an overview of the optimal control theory used including the problem definition and a description of the pseudospectral method. Section IV presents results validating the use of the pseudospectral method, optimal trajectory results for a range of maximum dynamic pressure conditions, and optimal trajectory results with variation in the vehicle's aerodynamic characteristics.

II. Problem Description

The simulated system includes a scramjet second stage, and a rocket powered third stage for payload delivery to heliosynchronous orbit. The airbreathing stage is assumed to be delivered to initial trajectory conditions by a first stage rocket which follows a fixed trajectory and has not been modelled. The following section details the models used for the second and third stages.

A. The Scramjet Accelerator

The Scramjet Powered Accelerator for Reusable Technology AdvaNcement (SPARTAN) is a scramjet powered accelerator under development by the University of Queensland to be used as the second stage in a scramjet-rocket powered system for delivering small payloads to heliosynchronous orbit, carrying a rocket stage in a recess on the top of the vehicle to reduce aerodynamic drag, as shown in Figure 1 [7, 18]. The SPARTAN is designed to be capable of flying back after separation to a designated landing point where recovery of the vehicle is possible without damage to the system. The SPARTAN is utilised in this study as a representative model for future multi-stage access to space systems incorporating airbreathing second stages.

The SPARTAN has a fuselage radius of 1.05m and has been sized to hold the third stage rocket and propellant tanks within the fuselage to reduce aerodynamic drag. Previous studies have indicated that using the SPARTAN as part of a three stage access to space system can produce

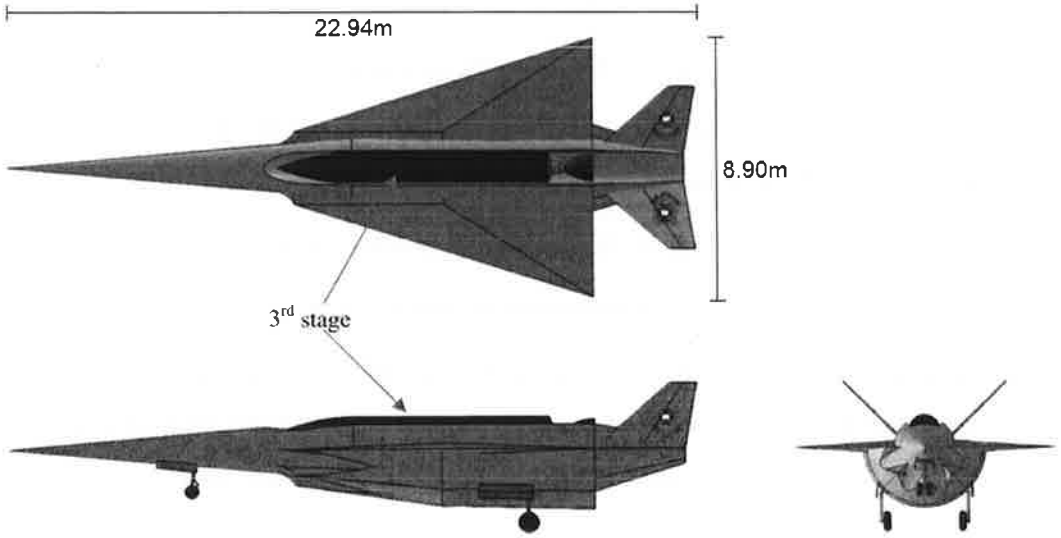

Fig. 1 CAD model of the SPARTAN accelerator [7].

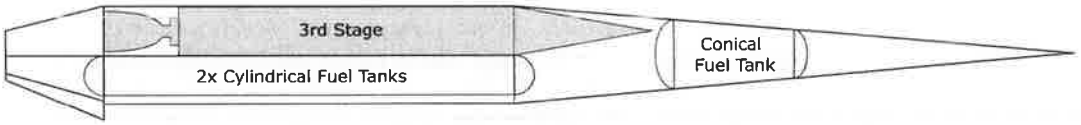

Fig. 2 Internal schematic view of the SPARTAN accelerator [7].

payload mass fractions that compare favourably with similarly sized rocket systems [7].

1. Dynamics Modelling

The aerodynamics of the SPARTAN are simulated using a set of aerodynamic data developed in HYPAERO [19]. HYPAERO utilises longitudinal strip theory to provide aerodynamic coefficients over the operating range of Mach numbers, angle of attacks and flap deflection angles of the vehicle. The SPARTAN is trimmed at all stages of the trajectory, utilising a simple golden sections method to optimise the flap deflection and angle of attack of the vehicle for trim with minimised drag [20]. The drag and lift produced by the vehicle are calculated using the standard definition of the aerodynamic coefficients:

$$F_d = \frac{1}{2}\rho c_d v^2 A, \tag{1}$$

$$F_L = \frac{1}{2}\rho c_L v^2 A. \tag{2}$$

With atmospheric properties drawn from the U.S. Standard Atmosphere 1976 [21]. The aerodynamic forces are integrated into horizontal and vertical position time histories through the equations of motion of the vehicle:

$$H = \int v \sin\theta dt, \tag{3}$$

$$V = \int v \cos\theta dt, \tag{4}$$

$$v = \int a dt, \tag{5}$$

$$\theta = \int \omega dt, \tag{6}$$

$$a = \frac{\sum F}{m}. \tag{7}$$

diagram show your definition of angles?

2. Scramjet Engine Modelling

The SPARTAN is powered by four scramjet engines located on the bottom portion of the fuselage, sized to a nominal capture width of 0.65m. These engines are based on the Rectangular-to-Elliptical Shape Transition (REST) scramjet engine design [22] with modified inlets to fit to a conical fuselage via a C-REST inlet configuration [23]. The engine model used is based on the RESTM12 database, a set of experimental data for a REST engine at off-design conditions [22], which provides data points of engine performance over inlet conditions within the operational range, at 50kPa dynamic pressure equivalent conditions. This data is interpolated for the given inlet conditions to calculate the exit conditions and the specific thrust T_s produced by the engine. The thrust T is then obtained by inclusion of the mass flow rate ($\dot{m}$) obtained via the inlet conditions, ie. $T = \dot{m}T_s$. Variation in dynamic pressure was accounted for by variation of $\dot{m}$ with air density ρ, with the assumption that engine efficiency is constant with ρ to a lower limit of $q = 20$kPa.

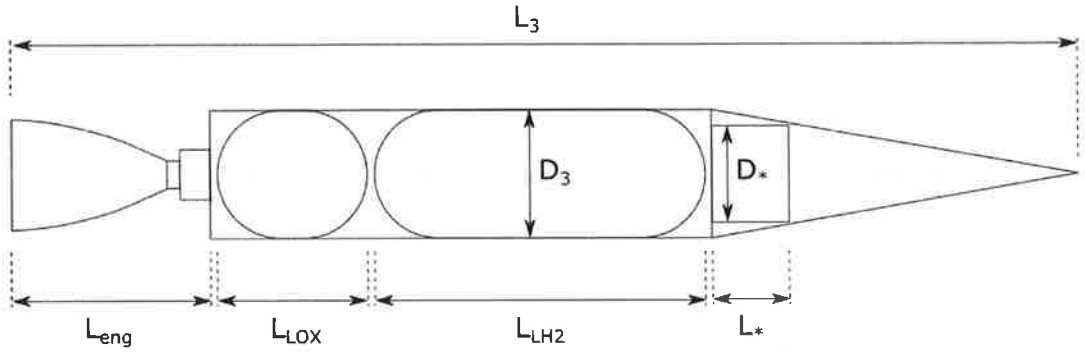

Fig. 3 Schematic of the third stage rocket [7].

B. The Rocket Stage

At the end of the SPARTAN acceleration, the rocket stage disengages, initiates burn, and performs an altitude increasing manoeuvre to achieve orbit. The rocket stage, shown in Figure 3, is modelled on the Pratt & Whitney RL-10A-3A, scaled to an engine mass of 100kg [7]. Scaled engine parameters are calculated by extrapolation of a statistical data set of 13 liquid hydrogen fuelled rocket motors [7]. The rocket dimensions, including fuel tanks, are dependent on the space available within the heat shield that envelopes the rocket. The payload is located at the nose of the rocket with a nominal size of $L_* = 0.075 L_{rocket}$ where $L_{rocket} = L_{eng} + L_{LOX} + L_{LH2} + 3L_{interface}$. The in-atmosphere separation of the rocket stage requires the use of a large heat shield that envelopes the rocket stage. The heat shield is constructed from Carbon-Carbon, weighing 302kg, and is discarded when the rocket has reached a dynamic pressure of 10Pa (atmospheric heating is assumed to be negligible at this point) [7].

The in-atmosphere portion of the rocket stage trajectory is simulated using CADac [24]. CADac is a set of simulation software developed for aircraft and spacecraft that simulates the trajectory until the rocket stage has achieved exoatmospheric flight, after which the final section of the payload delivery to heliosynchronous orbit is computed using simple Hohmann transfer equations [7]. The in-atmosphere trajectory of the rocket stage is a pull-up manoeuvre. This pull-up manoeuvre is simulated with constant angle of attack, which is optimised for given separation conditions to maximise payload mass to orbit. During the pull-up the axial and normal coefficients of the rocket

are calculated using [7]:

$$C_A = 0.346 + 0.183M - 0.058M^2 + 0.00382M^3, \tag{8}$$

$$C_N = (5.006 - 0.519M + 0.031M^2)\alpha, \tag{9}$$

and the lift and drag coefficients are calculated using [7]:

$$C_d = C_A \cos(\alpha) + C_N \sin(\alpha), \tag{10}$$

$$C_L = C_N \cos(\alpha) - C_A \sin(\alpha). \tag{11}$$

III. Trajectory Optimisation

In this paper the first rocket stage follows a fixed trajectory, which provides an initial separation state, from which the trajectory of the second stage scramjet vehicle and third stage rocket are designed. This separation point is given in Table 1.

Table 1 Second Stage Separation Conditions

Condition	Separation Point
Altitude	27km
Velocity	1864m/s
Dynamic Pressure	50kPa

so your analysis determines the initial flight path angle?

The second and third stages are simulated separately due to the relative simplicity of the rocket stage trajectory. This improves computational efficiency by allowing the optimisation of the second and third stages to be considered as two problems that are coupled by the second to third stage separation point ($\mathbf{x}_{2\to3}$):

- Determine the optimal trajectory of the second stage scramjet vehicle from first-second stage separation point ($\mathbf{x}_{1\to2}$) to $\mathbf{x}_{2\to3}$
- Determine the optimal trajectory for the third stage given $\mathbf{x}_{2\to3}$

Together these problems have the form of a sequential decision making problem, where the global optimal solution can be determined using dynamic programming [25]. For this specific problem, the

application of dynamic programming involves first determining the optimal value of payload for a range of feasible states $\mathbf{x}_{2\to3}$. A value function is computed efficiently by interpolating between states $\mathbf{x}_{2\to3}$, then this value function is treated as a terminal cost $C_3(\mathbf{x}_{2\to3})$. The optimal trajectory of the scramjet stage from $\mathbf{x}_{1\to2}$ to $\mathbf{x}_{2\to3}$ may be determined by selecting the control history $\mathbf{u}_2$:

$$\min_{\mathbf{u}_2} \quad C_2(\mathbf{x}_2, \mathbf{u}_2) + C_3(\mathbf{x}_{2\to3}), \tag{12}$$

where $C_2(\mathbf{x}_2, \mathbf{u}_2)$ is a second stage cost function and $\mathbf{x}_{2\to3}$ is dependent on the values of u_2 and x_2, ie. $\mathbf{x}_{2\to3} = g(u_2, x_2)$. The optimisation of Equation 12 subject to the vehicle dynamics has the form of a Bolza optimisation problem, where an objective function $J(\mathbf{u}, \mathbf{x}, \tau_f)$ is minimised,

$$J(\mathbf{u}(\tau), \mathbf{x}(\tau), \tau_f) = \underbrace{M[\mathbf{x}(\tau_f), \tau_f]}_{C_3(\mathbf{x}_{2\to3})} + \underbrace{\int_{\tau_0}^{\tau_f} P[\mathbf{x}(\tau), \mathbf{u}(\tau)]\, d\tau}_{C_2(\mathbf{x}_2, \mathbf{u}_2)}, \tag{13}$$

subject to a set of state dynamics $\dot{\mathbf{x}}(\tau)$, which describe the behaviour of the system over the solution space:

$$\dot{\mathbf{x}}(\tau) = f[\mathbf{x}(\tau), \mathbf{u}(\tau)]. \tag{14}$$

For the case of the aerodynamic simulation of the SPARTAN, the state dynamics correspond to the physical dynamics of the vehicle:

$$\dot{V} = v \sin\theta, \tag{15}$$

$$\dot{v} = a, \tag{16}$$

$$\dot{\theta} = \omega, \tag{17}$$

$$\dot{m} = -\dot{m}_{fuel}, \tag{18}$$

where the acceleration a and fuel mass flow rate $\dot{m}_{fuel}$ are given by the engine model. These dynamics are constrained by the boundary conditions of the system at the initial and final time points:

$$\psi_0[\mathbf{x}(\tau_0), \tau_0] = \mathbf{0}, \tag{19}$$

$$\psi_f[\mathbf{x}(\tau_f), \tau_f] = \mathbf{0}. \tag{20}$$

The dynamics are also subject to a set of inequality constraints defining the bounds of the problem:

$$\lambda[\mathbf{u}(t_k)] \leq \mathbf{0} \tag{21}$$

These bounds are chosen to span the possible operating range of the SPARTAN to ensure a globally optimal solution. Solving this Bolza problem in a discrete simulation requires the use of numerical solution methods for which the pseudospectral method solver DIDO has been chosen [26].

A. The Pseudospectral Method

The pseudospectral method is a form of direct collocation [17], which is a globally convergent method of solving partial differential equations (PDEs). The pseudospectral method offers good convergence properties and relatively good computational speed while not compromising the accuracy of the optimal solution [27]. These properties make the pseudospectral method appropriate for optimising a hypersonic vehicle system. The pseudospectral method utilises a spectral method approximation to convert the optimal control problem to be solved to PDE form. This method has been shown to be applicable to a variety of aerospace applications [12, 13, 28, 29].

The program LODESTAR (Launch Optimisation and Data Evaluation for Scramjet Trajectory Analysis Research) has been developed to produce an optimal trajectory path for the airbreathing stage of an orbital launch vehicle. LODESTAR utilises DIDO [26], a scramjet system simulation, and CADac [24], a third stage simulation module to produce an optimal trajectory. LODESTAR optimises a trajectory towards a customisable objective (i.e. constant dynamic pressures or optimal payload mass).

IV. Results and Discussion

LODESTAR was used to investigate the suitability of a pseudospectral method approach to global optimisation of scramjet-rocket trajectories. The following simulations were developed:

1. : $q = 50$kPa fixed trajectory $\rightarrow$ Verifies approach by comparison to previous results.

2. : Trajectory optimised for payload-to-orbit, q_{max} = 50kPa → Demonstrates the advantages of trajectory generation through coupled optimisation.

3. : Trajectory optimised for payload-to-orbit, q_{max} = 45kPa & q_{max} = 55kPa → Comparison of these simulations allows investigation into the effect of q max on payload-to-orbit.

4. : Trajectory optimised for payload-to-orbit, q_{max} = 50kpa, 110% Drag → Comparison of optimal trajectories at 100% and 110% drag allows investigation of the robustness of the solution with variation in vehicle design.

For all cases the starting point detailed in Table 1 is used. Table 2 details key results for comparison.

labels run into each other.

Table 2 Summary of Simulation Results

Trajectory Condition q	**50kPa Fixed**	**50kPa Limited**	**45kPa Limited**	**55kPa Limited**	**110% Drag**
Payload to Orbit (kg)	276.3	307.7	305.9	309.0	303.4
Separation Alt (km)	32.4	34.6	34.5	34.6	34.5
Separation v (m/s)	2850	2845	2828	2858	2805
Separation θ (deg)	0.23	2.86	2.86	2.86	2.86
Separation q (kPa)	50.0	35.5	35.2	35.8	34.9
Separation L/d	2.55	2.78	2.82	2.77	2.56
2^{nd} Stage Flight Time (s)	217.9	219.9	240.0	203.6	220.3
3^{rd} Stage Max q (kPa)	56.6	36.1	35.8	36.3	35.5
3^{rd} Stage $t >$ 20kpa (s)	39.5	27.1	27.3	27.0	27.6

A. Validation of LODESTAR

A constant dynamic pressure trajectory was produced for validation of LODESTAR compared to existing results. The trajectory was configured with a quadratic cost function centred around 50kPa dynamic pressure:

$$\min_{\mathbf{u}_2} \quad C_2(\mathbf{x}_2, \mathbf{u}_2) \tag{22}$$

$$C_2(\mathbf{x}_2, \mathbf{u}_2) = \int_{t_0}^{t_f} \frac{(q - 50 \times 10^3)^2 + 10^7}{10^7} dt \tag{23}$$

discuss flap deflection angle here, otherwise, why plot it?

The resulting constant dynamic pressure trajectory for the SPARTAN stage is shown in Figures 4, 5 and 6 with key results summarised in Table 2.

move figs 4, 5 & 6 to here.

too confusing for reader with them spread out

These results show very close adherence to 50kPa dynamic pressure (maximum 0.04% deviation) and close agreement with previous simulations of the SPARTAN vehicle controlled to q =50kPa using a Proportional-Integral-Derivative (PID) feedback controller [30]. The mean error in vertical trajectory position between LODESTAR and PID control [30] was found to be 0.46%, with a mean error in angle of attack of 1.11%. This close agreement indicates that LODESTAR is able to accurately simulate the scramjet vehicle throughout the trajectory.

Flying a constant dynamic pressure requires a low trajectory angle. This results in a third stage release angle of 0.23° to the horizontal. Over the 217.9 second trajectory the Mach no. increases from 6.0 to 9.4 and the velocity from 1798m/s to 2850m/s. The net specific impulse ($I_{sp_{net}} = \frac{T-F_d}{\dot{m}_f g}$) decreases over the trajectory, as the efficiency of the scramjet engines decreases. Hence the acceleration rate of the vehicle decreases significantly as the Mach number of the vehicle increases.

Figure 7 shows the corresponding third stage atmospheric exit trajectory after release at 50kPa, evaluated using CADac. After atmospheric exit, this trajectory is followed by a Hohmann transfer

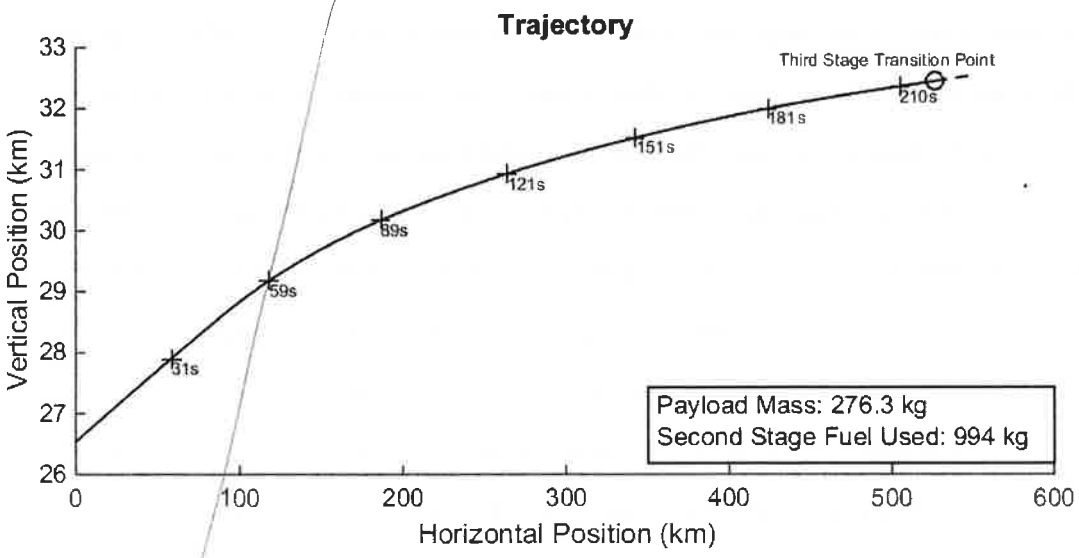

Fig7 here!

Fig. 4 Trajectory path of the 2^{nd} stage SPARTAN vehicle flying at 50kPa constant dynamic pressure.

you have not described how you chose α=13°. Readers need a little more here. Did you allow variable α during pull-up? Needs clarity and figures adjacent to text.

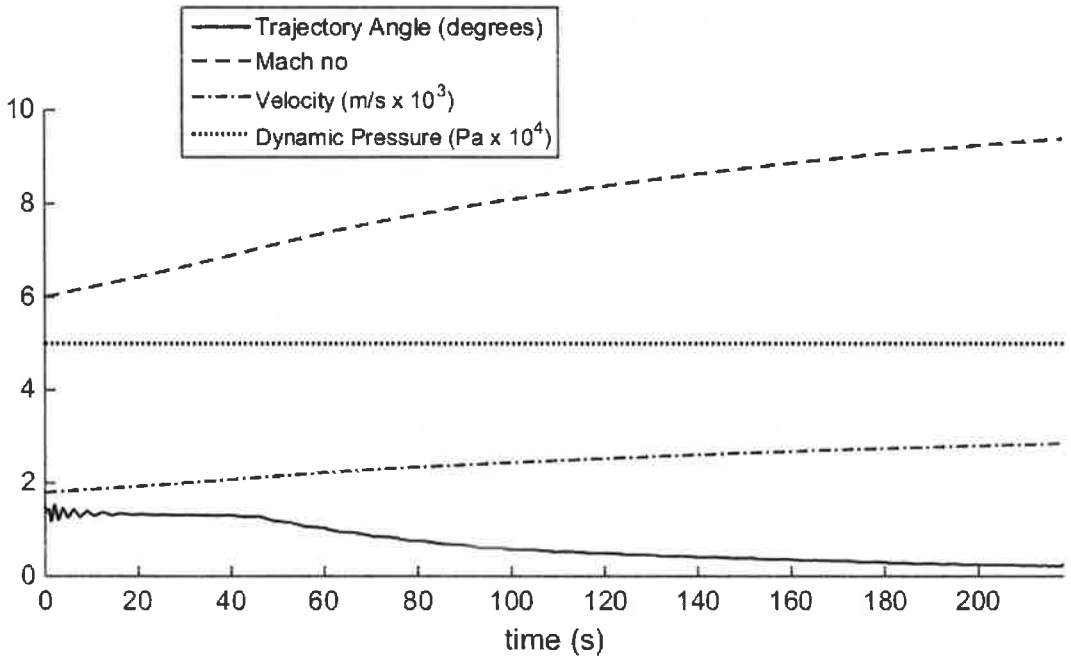

Fig. 5 Trajectory data for 50kPa constant dynamic pressure trajectory.

to a heliosynchronous orbit, resulting in a total payload to orbit of 276.3kg.

B. Third Stage Evaluation

In order to increase the computational efficiency of the optimisation, it was decided to consider the third stage rocket as an end point cost of the scramjet stage trajectory, as opposed to optimising the entirety of the trajectory at once. The third stage rocket trajectory was simulated over a variety of separation conditions using CADac. Payload to orbit ($C_3(\mathbf{x}_{2\to3})$) was calculated over a 3D grid of separation conditions $(V_{2\to3}, v_{2\to3}, \theta_{2\to3})$, with selected velocity conditions shown in Figure 8.

The results indicate that the payload mass to orbit increases universally as separation velocity is increased, with maximum payload to orbit achieved at a separation of 40km altitude and 0° trajectory angle at 3000m/s. For all velocity conditions maximum payload occurs at high altitude and between 0°-2° trajectory angle. Although achieving close to 40km altitude may not be viable as the atmosphere becomes unable to sustain efficient flight. As the scramjet engines provide less thrust in low dynamic pressure, less acceleration is possible when manoeuvring to higher altitudes, creating a trade-off between the velocity able to be achieved and the altitude of separation. Figure 8 shows

Is θ the same as AOA?

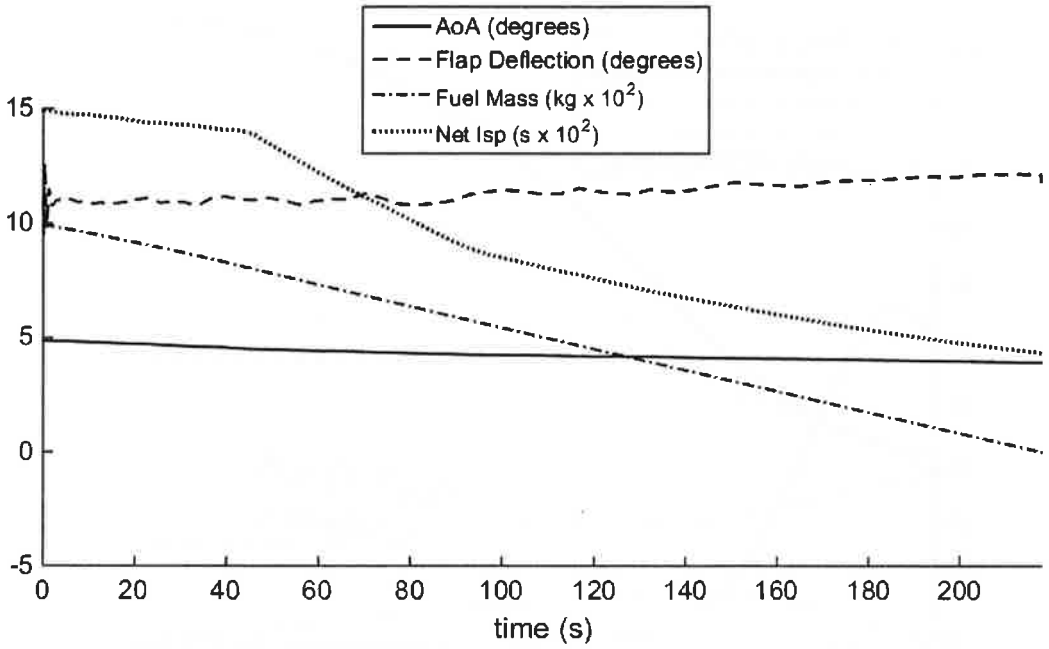

Fig. 6 Vehicle performance data for 50kPa constant dynamic pressure trajectory. Note: Flap deflection is positive down.

distinct maximum regions and indicates that as the altitude of separation decreases, the optimal trajectory angle increases. The observed trend is a consequence of the interaction between rocket aerodynamic efficiency and the time spent inside the atmosphere at high density. When released at higher altitude the rocket has a smaller atmospheric exit pull-up manoeuvre to complete and lower drag when compared to a low altitude release. Hence, at high altitudes it is preferable for the rocket to be released at a lower trajectory angle to allow the rocket greater tangential acceleration. The resultant tangential velocity is used to assist in increasing the altitude of the rocket, increasing overall efficiency.

C. Dynamic Pressure Limited Trajectory

LODESTAR was configured to optimise the total payload mass to orbit:

$$\min_{\mathbf{u}_2} \quad C_2(\mathbf{x}_2.\mathbf{u}_2) + C_3(\mathbf{x}_{2\to 3}) \tag{24}$$

where

$$C_2(\mathbf{x}_2, \mathbf{u}_2) = 0.01 \int_{t_0}^{t_f} \dot{m}_f dt \tag{25}$$

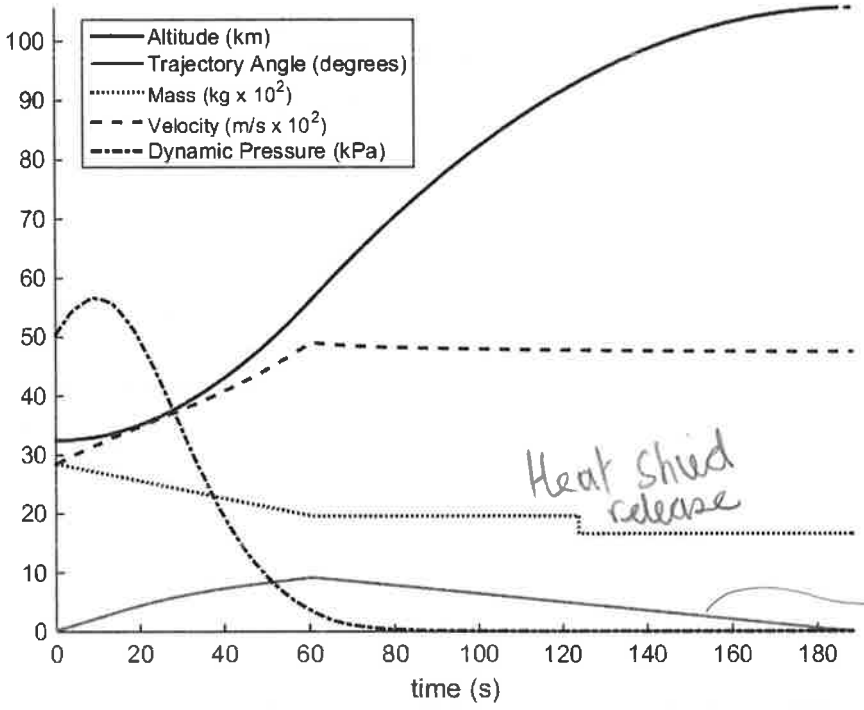

don't assume colour.

Fig. 7 Third stage rocket trajectory simulated from the end of the 50kPa constant dynamic pressure SPARTAN trajectory. Flown at an optimal α of $13.0°$.

$$C_3(\mathbf{x}_{2\to 3}) = -m_{payload} \tag{26}$$

In this case $C_3(\mathbf{x}_{2\to 3})$ is the trajectory target and is determined via interpolation of the third stage release point grid. $C_2(\mathbf{x}_2, \mathbf{u}_2)$ is included to improve numerical stability and has been chosen to have negligible effect on the resultant trajectory.

A maximum dynamic pressure limit of 50kPa was applied to the optimisation process to allow direct comparison with the constant q trajectory and so that the equivalent vehicle can be used. This trajectory was limited to 0.05 radians (2.86°) maximum trajectory angle to capture a conservative estimate of vehicle capabilities, ie. a trajectory that is within the acceptable operating region of the SPARTAN. The initial conditions were constrained as shown in Table 1, all other factors were computed entirely in the optimisation routine.

adjacent figs all on one page

The optimal trajectory shape for a q =50kPa limited, maximum payload to orbit trajectory is shown in Figures 9, 10 and 11 with key results summarised in Table 2. The trajectory follows a constant dynamic pressure path at 50kPa for the first 201.7s of flight, after which a pull-up

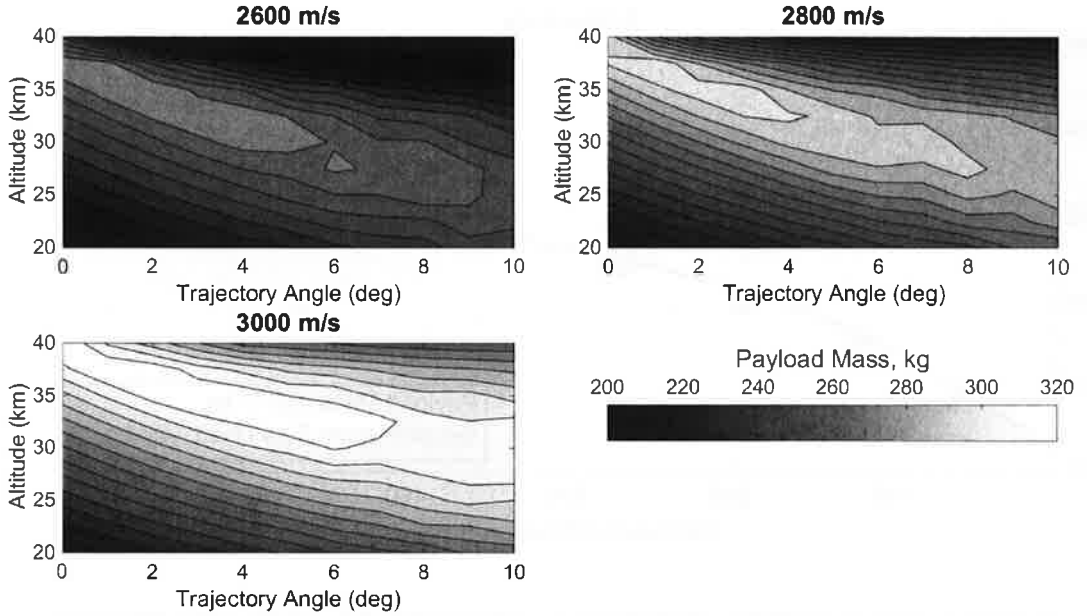

Fig. 8 Payload mass results with variation in rocket stage release point at 2600m/s, 2800m/s and 3000m/s velocity conditions. Produced using CADac ~~as a LODESTAR module~~.

manoeuvre is performed, gaining altitude at maximum inclination until rocket stage release at 219.9s flight time. This trajectory is able to deliver 307.7kg of payload to heliocentric orbit, an increase of 11.4% over the constant dynamic pressure result. The point at which the pull-up manoeuvre begins is the optimisation result that takes into account the best combination of v, altitude and release angle for scramjet stage performance and the release of the rocket stage. The constant rate of climb at the end of trajectory indicates the region at which increasing altitude and release angle becomes more important than extracting maximum thrust from the scramjet (which is attained at high q, low flight angle). Flight in a lower dynamic pressure environment results in less thrust output from the scramjet engines, as well as an increase in angle of attack and flap deflection angle to compensate for the additional lift required. Due to this, less overall acceleration is obtained compared to the constant dynamic pressure result. Separation occurs at a velocity of 2845m/s, a decrease of 5m/s. However, separation altitude increases by 2.2km to 34.6km, resulting in a decreased separation dynamic pressure of 35.5kPa.

The scramjet stage pull-up assists the rocket in manoeuvring to exoatmospheric altitude by

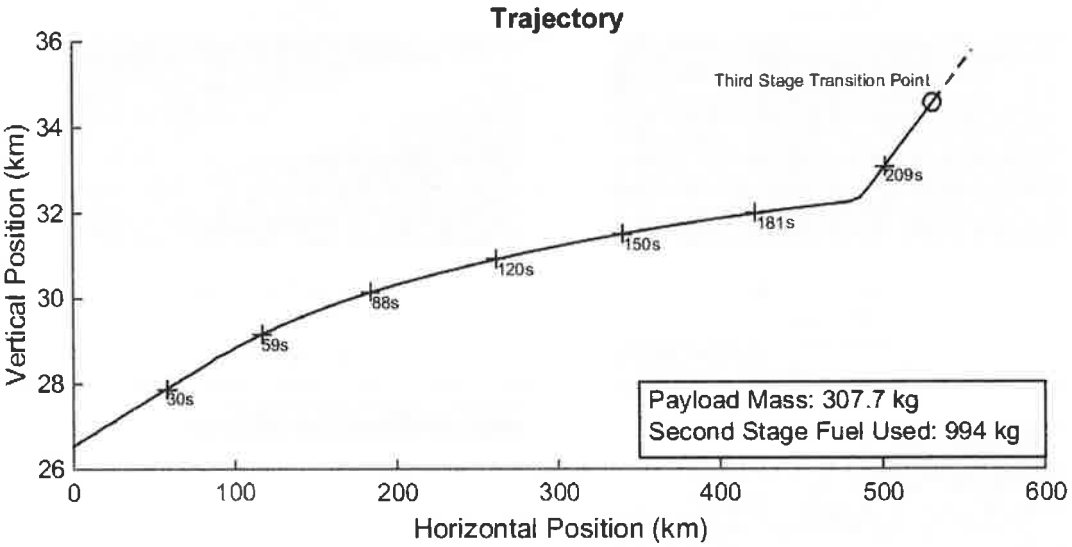

Fig. 9 Maximum payload trajectory path of the 2^{nd} stage SPARTAN vehicle when limited to 50kPa dynamic pressure.

increasing the altitude and angle at separation by virtue of the increased L/d ratio and manoeuvrability of the scramjet vehicle. Even a small release angle of 2.86° significantly reduces the turning that is required by the rocket as evident from comparing Fig 7 and 12, lessening the time that the rocket must spend in a high dynamic pressure environment, and decreasing the maximum dynamic pressure that the rocket stage experiences by 36.2%, as shown in Table 2.

Compared to studies considering vehicles with a scramjet-rocket transition within a single stage [9][10], the maximum payload to orbit trajectory of the multi-stage system shows a scramjet-rocket transition point at much lower altitudes. This lower transition point is a consequence of the stage separation creating an energy trade-off which does not occur in a single stage vehicle. In the multi-stage system, the optimal separation point is dependent on utilising the superior aerodynamic performance and engine efficiency of the scramjet stage, while trading-off the energy cost of increasing the altitude of the scramjet stage. Past a certain point, the energy required to increase the altitude of the scramjet stage is not offset by the performance benefits, and staging occurs. This beneficial ability to separate the scramjet stage results in a lower scramjet-rocket transition point when compared to single stage vehicle designs. Single stage vehicles must necessarily transport all components to exoatmosphere, and so utilise the scramjet engines until higher altitude to take

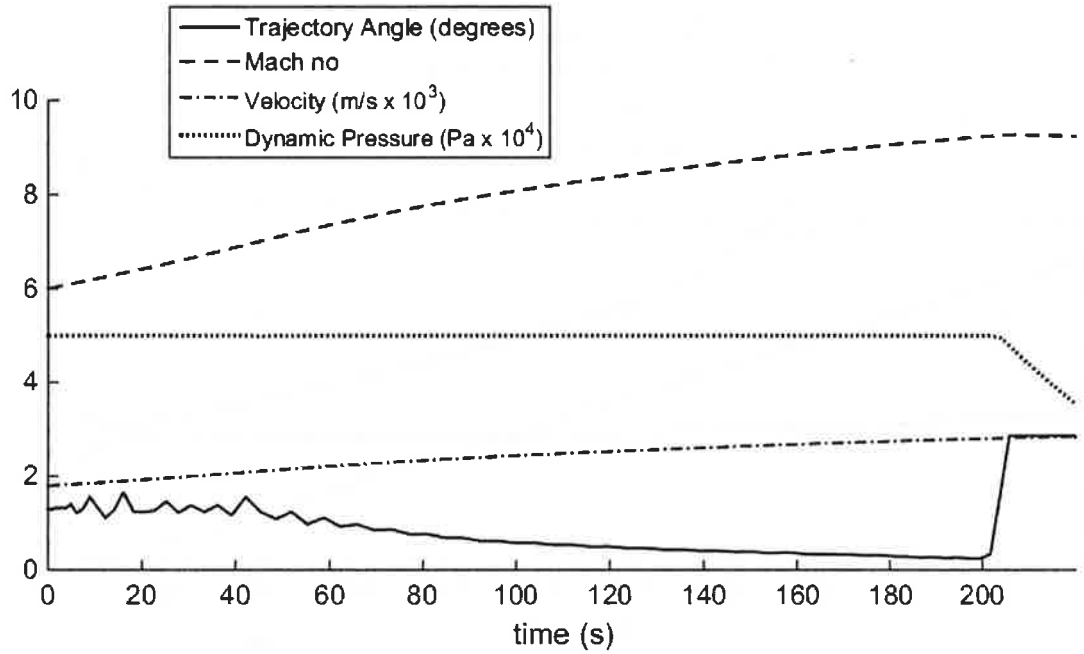

Fig. 10 Trajectory data for 50kpa dynamic pressure limited trajectory.

advantage of their high efficiency.

D. Dynamic Pressure Sensitivity

To investigate the sensitivity of the vehicle to changes in q_{max}, the maximum dynamic pressure was varied to 45kPa and 55kPa and the flight trajectory optimised, with results shown in Figures 13, 14 and 15 and summarised in Table 2. The $\pm 10\%$ variation in maximum dynamic pressure has been shown to have very little effect on the payload mass delivered to heliocentric orbit. Varying the maximum dynamic pressure by $\pm$5kPa from the 50kPa base q causes a variation of only +1.3kg (0.42%) or $-$1.8kg (0.58%).

Both trajectories use 994kg of fuel and reach similar separation altitudes of 34.5km and 34.6km with separation velocities of 2828m/s and 2858m/s for 45kPa and 55kPa respectively. The small variation in separation velocity indicates that the maximum dynamic pressure of the vehicle does not have a large impact on the total acceleration of the vehicle. This small variation in velocity is despite the increase in air density and decrease in angle of attack with increased maximum dynamic pressure, both of which increase the mass flow into the engine. Although the thrust

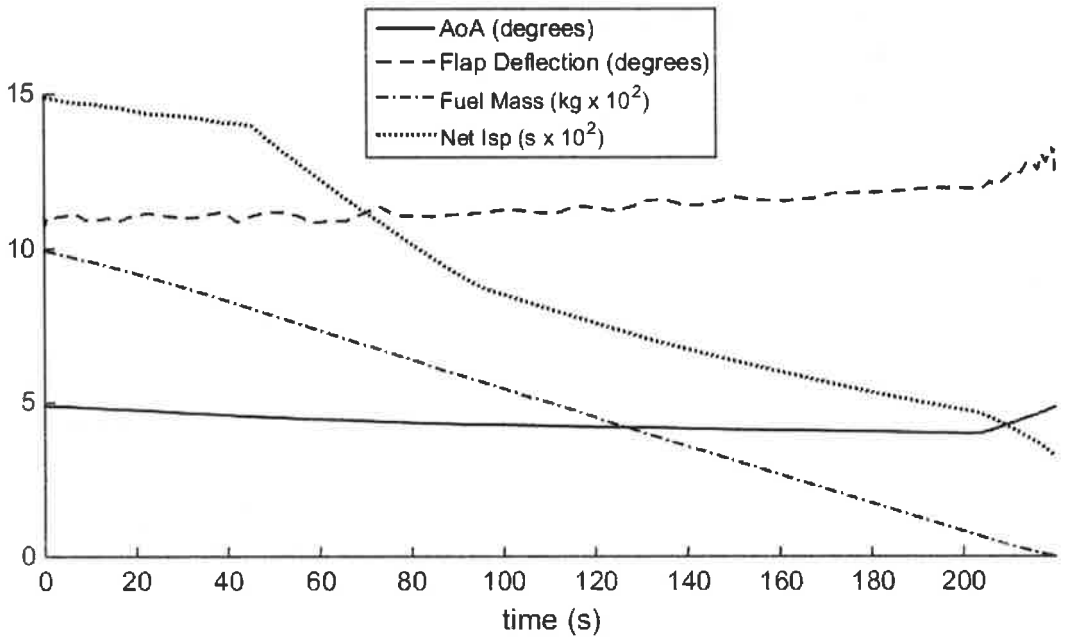

Fig. 11 Vehicle performance data for 50kpa dynamic pressure limited trajectory. Note: Flap deflection is positive down.

output of the REST engines increases with dynamic pressure, so does the drag on the vehicle, and the increased performance is minimal. Both trajectories reach similar altitudes for third stage separation, however the 55kpa trajectory requires a larger pull-up manoeuvre to reach the separation point. This similarity in separation points indicates that reaching optimal separation altitude is preferred over increased acceleration in the scenarios tested.

Minimal variation in optimal separation conditions has been observed, without modification of vehicle design to account for dynamic pressure limit. This indicates that designing and operating a vehicle at lower dynamic pressures may be preferable. Flying at a lower maximum dynamic pressure allows reduction of the structural weight and heat shielding of the vehicle. Additionally, flying at low dynamic pressure requires a shorter pull-up, resulting in less dynamic pressure variation. The 45kPa limited trajectory reaches a minimum of 35.2kPa, a variation of 9.8kPa, compared to the 55kpa limited trajectory which reaches a minimum of 35.8kPa, a variation of 19.2kPa. If the vehicle is to be designed to a specific dynamic pressure limit, the reduced dynamic pressure range of the 45kPa limit is beneficial for scramjet engine design, as the scramjets will be operated closer to their

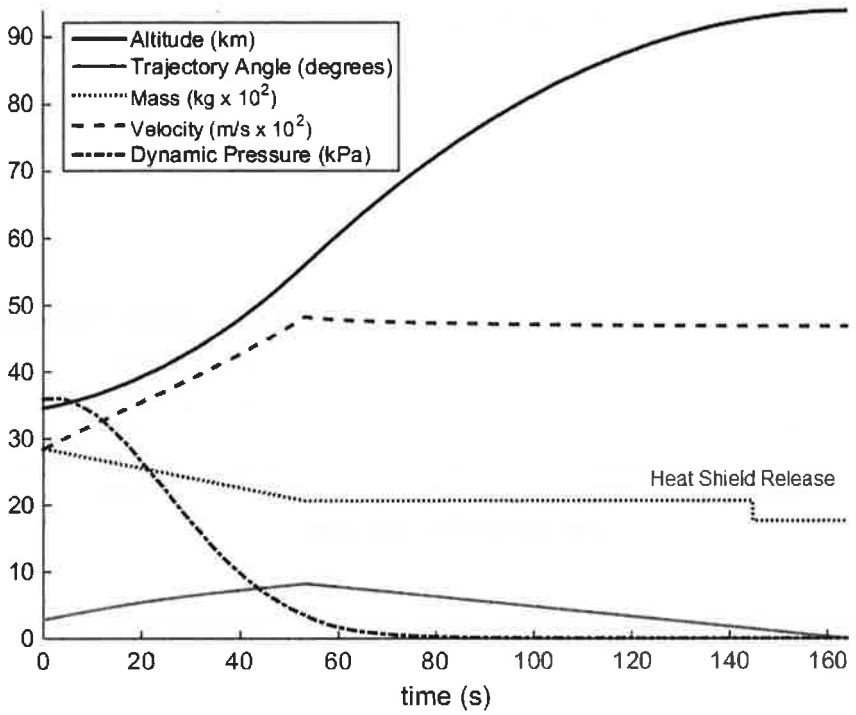

Fig. 12 Third stage rocket trajectory simulated from the end of the 50kPa dynamic pressure limited maximum payload SPARTAN trajectory. Flown at an optimal α of 12.7°.

intended design point throughout the pull-up manoeuvre.

E. Lift/Drag Ratio Sensitivity Analysis

To investigate the effect of vehicle design and uncertainty in aerodynamic performance on the optimal trajectory the drag on the vehicle was increased by 10%, and an optimised trajectory calculated with dynamic pressure limited to 50kpa. Selected results are compared to the baseline q =50kPa limited result in Figures 16 and 17. These results show that when drag is increased (ie. L/d is decreased) the high drag second stage lags behind the base-line trajectory and follows a slightly slower and hence lower flight path. However at the end the pull-up manoeuvre is initialised earlier resulting in a 3rd stage release point that is only slight slower (2805 m/s, a 1.4% reduction) and lower (34.5km, compared to 34.6km). The net result is a lower payload-to-orbit of 303.4kg (a decrease of 1.4%). Though the separation point varies, the shape of the pull-up manoeuvre that occurs for the increased drag case is very similar to that of the baseline case. This similarity

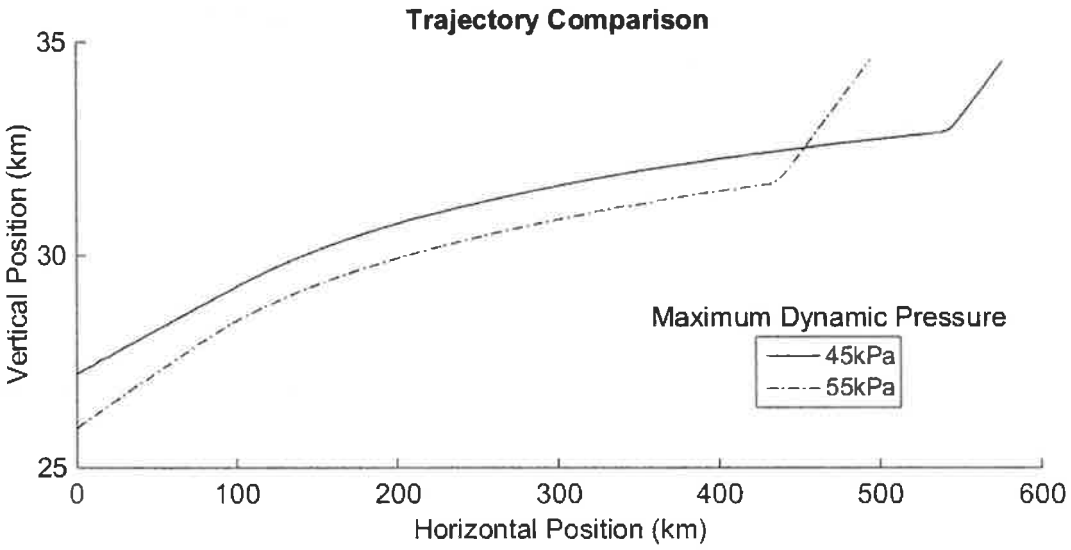

Fig. 13 Comparison of 45kPa / 55kpa dynamic pressure limited trajectory paths for maximum payload to orbit.

suggests that a pull-up manoeuvre is optimal for multiple vehicle designs. Additionally, the similar payload-to-orbit results indicate that re-optimisation of the trajectory is an effective way to mitigate the effects of significant changes in vehicle design, although so far only the effect of second stage vehicle drag on payload to orbit has been investigated. The results have shown that the net impact of increased scramjet stage drag on the payload to orbit is rather small, particularly if one considers that the highest drag losses occur during the second stage flight.

V. Conclusions

In this paper an optimal control program, LODESTAR, has been used to optimise the trajectory of a scramjet-rocket multi-stage system. LODESTAR has been validated against traditional feedback control and has been shown to be able to generate globally optimised trajectory simulations leading to increased performance of the multi-stage system.

← sentences describing SPARTAN

Results indicate that a pull-up manoeuvre at the end of a constant dynamic pressure trajectory is the optimal scramjet flight path for a system transitioning between separate airbreathing and rocket-powered stages. Using the SPARTAN vehicle as a model, the globally optimal flight trajectory was found to produce an increase of 11.4% in payload mass to heliocentric orbit, and a decrease of

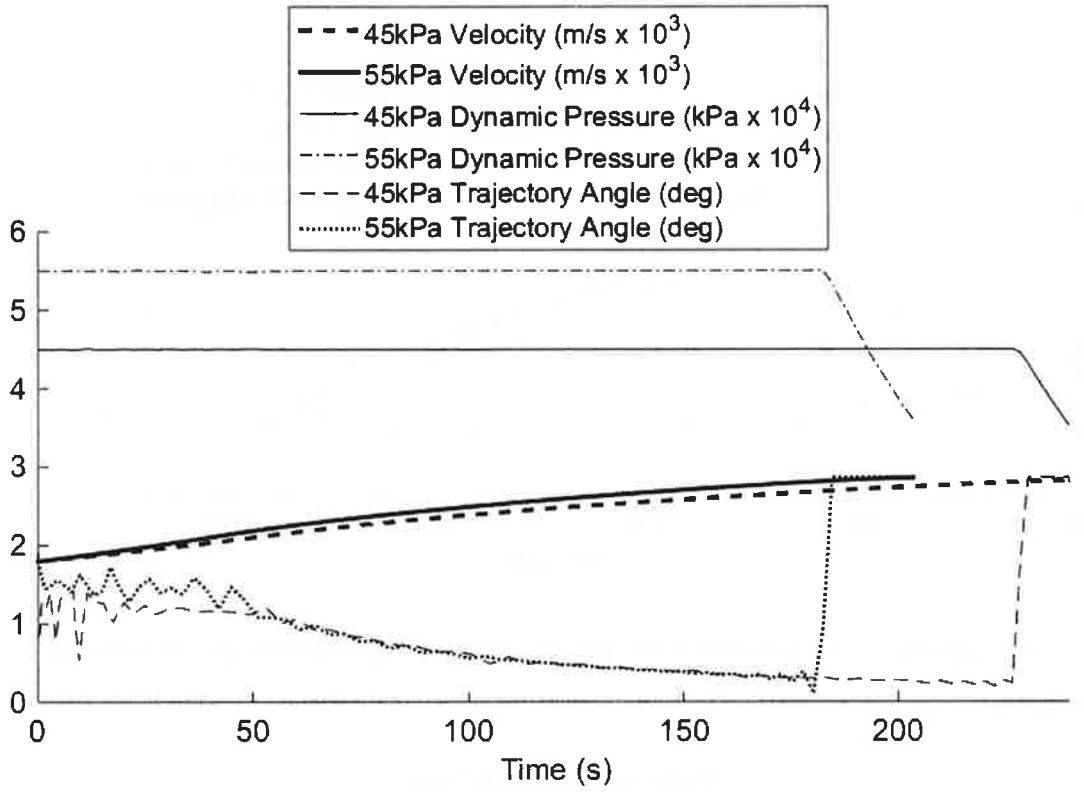

Fig. 14 Comparison of trajectory data for 45kPa / 55kpa dynamic pressure limited trajectories.

36.2% in the maximum dynamic pressure experienced by the rocket-powered stage. This decrease in maximum dynamic pressure decreases the stress experienced by the rocket stage proportionally, as well as decreasing the heat flux into the rocket, both of which lead to significant benefits for the design of the rocket stage. A decrease in structural stress allows for less internal reinforcement, and a decrease in heat flux allows for reduction of the heat shield size, resulting in further increases in payload mass.

As part of a dynamic pressure sensitivity evaluation, the maximum dynamic pressure limit of the vehicle was varied by ±5kPa. This was found to produce only a +0.42% and −0.58% variation on the payload mass delivered to orbit. This small variation in payload-to-orbit indicates that a scramjet powered stage designed for operation at lower q may be advantageous. If efficient, low q scramjet engines are available, operating at lower q enables lighter vehicles due to reduced structural and thermal loads. This reduction in mass potentially leads to further performance improvements

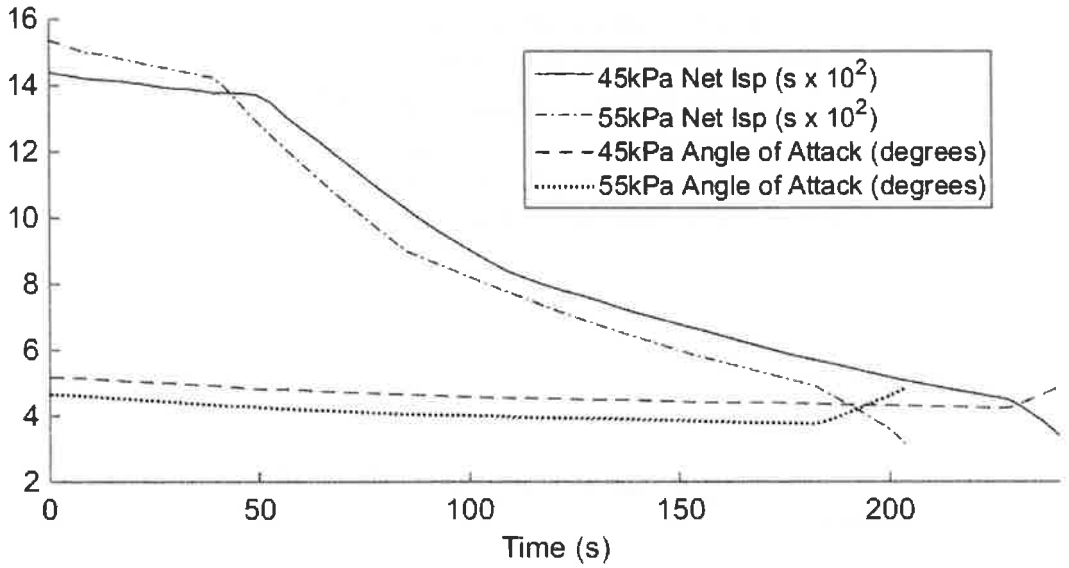

Fig. 15 Comparison of vehicle performance data for 45kPa / 55kpa dynamic pressure limited trajectories.

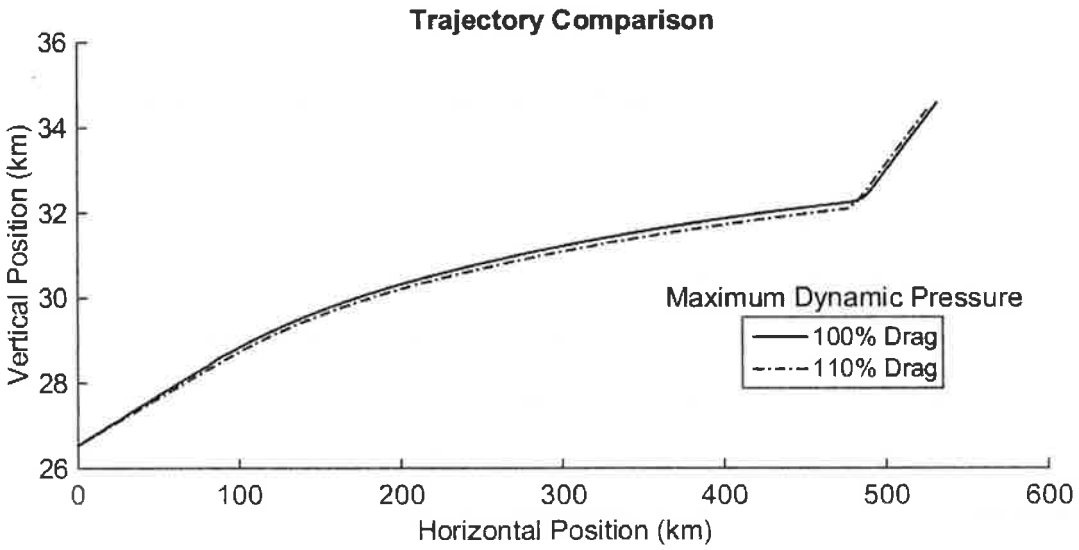

Fig. 16 Comparison of trajectory paths for 100% and 110% drag cases for a 50kPa dynamic pressure limited maximum payload trajectory.

and operational benefits including increased payload to orbit and extended range.

To investigate the effect of changes in second stage vehicle properties, the drag of the scramjet was increased by 10% and the optimal trajectory evaluated. It was found that a pull-up manoeuvre

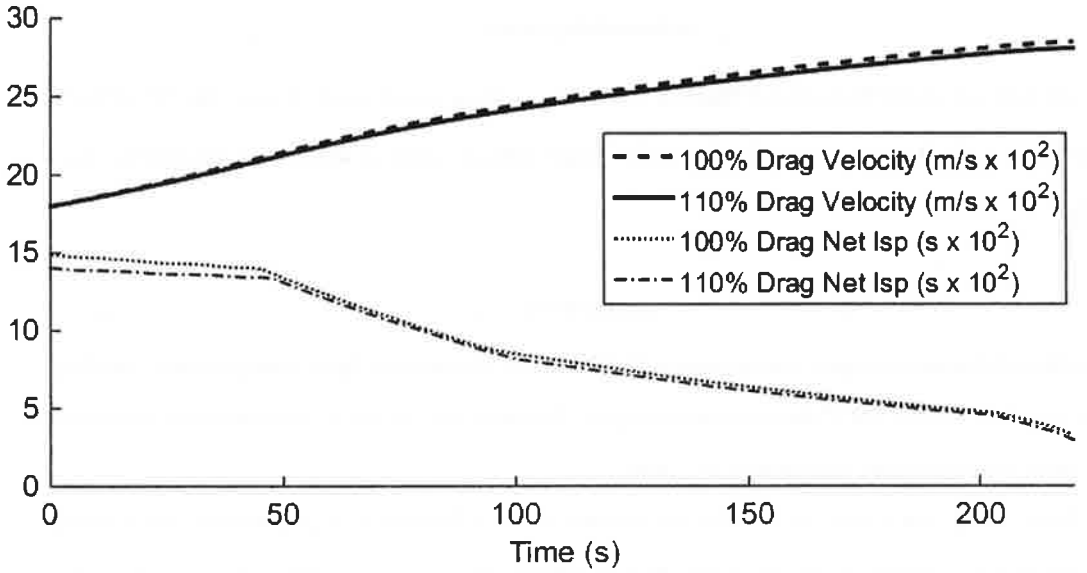

Fig. 17 Comparison of v and $I_{sp_{net}}$ for 100% and 110% drag cases for a 50kPa dynamic pressure limited maximum payload trajectory.

occurred with a lower first-second stage transition point when compared to the original result, indicating that the rocket is favoured at an earlier point in the climb manoeuvre. This variation in the optimal trajectory was minor, indicating that the trajectory shape presented is robust with respect to changes in vehicle design and, by extension, changes in engine performance. Thus re-optimisation of the trajectory while taking account of the new aerodynamic performance is a good approach to minimise impacts on the aggregate performance of the system.

Overall this work has provided new insight into the preferred operating capabilities for scramjet vehicles incorporated in multi-stage to orbit systems.

VI. Future Work

Analysis is under way to increase the fidelity of the SPARTAN model, and to extend the range of flight conditions over which it is able to be accurately simulated. Inclusion of the first stage trajectory simulation, updates to the third stage trajectory design, and the incorporation of parametric design into the optimisation process are projected to further increase the payload mass fraction to orbit.

Acknowledgments

The authors would like to thank Dawid Preller for providing aerodynamic data on the SPARTAN vehicle and a CADac simulation for the rocket stage vehicle, both of which were integral to this study.

References

[1] Office of Commercial Space Transportation (AST) and the Commercial Space Transportation Advisory Committee (COMSTAC). *2001 Commercial Space Transportation Forecasts.* May, Office of Commercial Space Transportation, Washington, DC, 2001.

[2] Smart, M. K. and Tetlow, M. R. "Orbital Delivery of Small Payloads Using Hypersonic Airbreathing Propulsion." *Journal of Spacecraft and Rockets*, volume 46(1), 117–125, 2009. ISSN 0022-4650. doi: 10.2514/1.38784.

[3] Heiser H. H. and Pratt, D. T. *Hypersonic Airbreathing Propulsion.* American Institute of Aeronautics and Astronautics, Washington, D.C, 1994. ISBN 1-56347-035-7. doi:10.2514/4.470356.

[4] Flaherty, K. W., Andrews, K. M., and Liston, G. W. "Operability Benefits of Airbreathing Hypersonic Propulsion for Flexible Access to Space." *Journal of Spacecraft and Rockets*, volume 47(2), 280–287, 2010. ISSN 0022-4650. doi:10.2514/1.43750.

[5] Kimura, T. and Sawada, K. "Three-Stage Launch System with Scramjets." *Journal of Spacecraft and Rockets*, volume 36(5), 675–680, 1999. ISSN 00224650. doi:10.2514/2.3500.

[6] Olds, J. and Budianto, I. "Constant Dynamic Pressure Trajectory Simulation with POST." In "Aerospace Sciences Meeting & Exhibit," Reno, NV, 1998, pages 1–13. doi:10.2514/6.1998-302.

[7] Preller, D. and Smart, M. K. "Scramjets for Reusable Launch of Small Satellites." In "20th AIAA International Space Planes and Hypersonic Systems and Technologies Conference," July, Glasgow, Scotland, 2015, pages 1–23. doi:10.2514/6.2015-3586.

[8] Powell, R. W., Shaughnessy, J. D., Cruz, C. I., and Naftel, J. C. "Ascent performance of an air-breathing horizontal-takeoff launch vehicle." volume 14(4), 834–839, 1991. ISSN 0731-5090. doi:10.2514/3.20719.

[9] Lu, P. "Inverse dynamics approach to trajectory optimization for an aerospace plane." *Journal of Guidance, Control, and Dynamics*, volume 16(4), 726–732, 1993. ISSN 0731-5090. doi:10.2514/3.21073.

[10] Trefny, C. "An Air-Breathing Concept Launch Vehicle for Single-Stage-to-Orbit." In "35th Joing Propulsion Conference and Exhibit," May, Los Angeles, CA, 1999.

[11] Mehta, U. B. and Bowles, J. V. "Two-Stage-to-Orbit Spaceplane Concept with Growth Potential." *Journal of Propulsion and Power*, volume 17(6), 1149–1161, 2001. ISSN 0748-4658. doi:10.2514/2.5886.

[12] Bedrossian, N., Technologies, B., and Nasa, L. N. "Zero Propellant Maneuvre Flight Results For 180 Degree ISS Rotation." In "20th International Symposium on Space Flight Dynamics," Annapolis, MD, 2007.

[13] Josselyn, S. and Ross, I. M. "Rapid Verification Method for the Trajectory Optimization of Reentry Vehicles." *Journal of Guidance, Control, and Dynamics*, volume 26(3), 505–508, 2002. ISSN 0731-5090. doi:10.2514/2.5074.

[14] Sekhavat, P., Fleming, A., and Ross, I. "Time-optimal nonlinear feedback control for the NPSAT1 spacecraft." In "Proceedings, 2005 IEEE/ASME International Conference on Advanced Intelligent Mechatronics.", Monterey, CA, 2005, pages 24–28. ISBN 0-7803-9047-4. doi:10.1109/AIM.2005.1511114.

[15] Ranieri, C. L. and Ocampo, C. a. "Optimization of Roundtrip, Time-Constrained, Finite Burn Trajectories via an Indirect Method." *Journal of Guidance, Control, and Dynamics*, volume 28(2), 306–314, 2005. ISSN 0731-5090. doi:10.2514/1.5540.

[16] Elnagar, G., Kazemi, M. a., and Razzaghi, M. "The Pseudospectral Legendre Method for Discetizing Optimal Control Problems." *IEEE Transactions on Automatic Control*, volume 40(10), 1793–1796, 1995.

[17] Fahroo, F. and Ross, I. "Direct trajectory optimization by a Chebyshev pseudospectral method." In "Proceedings of the 2000 American Control Conference.", Chicago, IL, 2000, volume 6, pages 3860–3864. ISBN 0-7803-5519-9. ISSN 0743-1619. doi:10.1109/ACC.2000.876945.

[18] Jazra, T., Preller, D., and Smart, M. K. "Design of an Airbreathing Second Stage for a Rocket-Scramjet-Rocket Launch Vehicle." *Journal of Spacecraft and Rockets*, volume 50(2), 411–422, 2013. ISSN 0022-4650. doi:10.2514/1.A32381.

[19] Jazra, T. and Smart, M. "Development of an Aerodynamics Code for the Optimisation of Hypersonic Vehicles." In "47th AIAA Aerospace Sciences Meeting Including The New Horizons Forum and Aerospace Exposition," Orlando, Florida, 2009, page 2009. doi:10.2514/6.2009-1475.

[20] Kiefer, J. "Sequential Minimax Search for a Maximum." *Proceedings of the American Mathematical Society*, volume 4(3), 502–506, 1953.

[21] NASA. *U.S. Standard Atmosphere, 1976*. U.S. Government Printing Office, Washington, D.C., 1976.

[22] Suraweera, M. and Smart, M. K. "Shock Tunnel Experiments with a Mach 12 {REST} Scramjet at Off-Design Conditions." *Journal of Propulsion and Power*, volume 25(3), 555 564, 2009. ISSN 0748-4658. doi:10.2514/1.37946.

[23] Gollan, R. J. and Smart, M. K. "Design of Modular , Shape-transitioning Inlets for a Conical Hypersonic Vehicle." *Aerospace, AIAA*, volume 29(4), 832 838, 2013. ISSN 0748-4658. doi:10.2514/6.2010-940.

[24] Zipfel, P. H. *Modeling and Simulation of Aerospace Vehicle Dynamics, Second Edition.* American Institute of Aeronautics and Astronautics, Reston, VA, 2007. ISBN 978-1-56347-875-8. doi:10.2514/4.862182.

[25] Bertsekas, D. P. *Dynamic Programming and Optimal Control, Volume I.* Athena Scientific, Belmont, MA, 2005. ISBN 1886529264.

[26] Ross, I. M. *A Beginners Guide to DIDO (ver 7.3): A MATLAB Application Package for Solving Optimal Control Problems.* Elissar, LLC, Monterey, CA.

[27] Fasano, G. and Pinter, J. *Modelling and Optimisation in Space Engineering.* Springer, New York, NY, 2013. doi:10.1007/978-1-4614-4469-5.

[28] Huntington, G. T. and Rao, A. V. "Optimal Reconfiguration of Spacecraft Formations Using the Gauss Pseudospectral Method." *Journal of Guidance, Control, and Dynamics*, volume 31(3), 689–698, 2008. ISSN 0731-5090. doi:10.2514/1.31083.

[29] Yan, H., Ross, I. M., and Alfriend, K. T. "Pseudospectral Feedback Control for Three-Axis Magnetic Attitude Stabilization in Elliptic Orbits." *Journal of Guidance, Control, and Dynamics*, volume 30(4), 1107–1115, 2007. ISSN 0731-5090. doi:10.2514/1.26591.

[30] Preller, D. and Smart, M. K. "Longitudinal Control Strategy for Hypersonic Accelerating Vehicles." *Journal of Spacecraft and Rockets*, volume 52(3), 1–6, 2015. ISSN 0022-4650. doi:10.2514/1.A32934.